Description of the Mass Spectrometer for the Jupiter Icy Moons Explorer Mission

Martina Föhn
University of Bern, Physics Institute
Sidlerstrasse 5
3012 Bern
martina.foehn@space.unibe.ch

André Galli
University of Bern, Physics Institute
Sidlerstrasse 5
3012 Bern
andre.galli@space.unibe.ch

Audrey Vorburger
University of Bern, Physics Institute
Sidlerstrasse 5
3012 Bern
audrey.vorburger@space.unibe.ch

Marek Tulej
University of Bern, Physics Institute
Sidlerstrasse 5
3012 Bern
marek.tulej@space.unibe.ch

Davide Lasi
University of Bern, Physics Institute
Sidlerstrasse 5
3012 Bern
davide.lasi@space.unibe.ch

Andreas Riedo
University of Bern, Physics Institute
Sidlerstrasse 5
3012 Bern
andreas.riedo@space.unibe.ch

Rico G. Fausch
University of Bern, Physics Institute
Sidlerstrasse 5
3012 Bern
rico.fausch@space.unibe.ch

Michael Althaus
University of Bern, Physics Institute
Sidlerstrasse 5
3012 Bern
michael.althaus@space.unibe.ch

Stefan Brüngger
University of Bern, Physics Institute
Sidlerstrasse 5
3012 Bern
stefan.bruengger@space.unibe.ch

Philipp Fahrer
University of Bern, Physics Institute
Sidlerstrasse 5
3012 Bern
philipp.fahrer@space.unibe.ch

Michael Gerber
University of Bern, Physics Institute
Sidlerstrasse 5
3012 Bern
michael.gerber@space.unibe.ch

Matthias Lüthi
University of Bern, Physics Institute
Sidlerstrasse 5
3012 Bern
luethi@space.unibe.ch

Hans Peter Munz
University of Bern, Physics Institute
Sidlerstrasse 5
3012 Bern
hanz-peter.munz@space.unibe.ch

Severin Oeschger
University of Bern, Physics Institute
Sidlerstrasse 5
3012 Bern
severin.oeschger@space.unibe.ch

Daniele Piazza
University of Bern, Physics Institute
Sidlerstrasse 5
3012 Bern
daniele.piazza@space.unibe.ch

Peter Wurz
University of Bern, Physics Institute
Sidlerstrasse 5
3012 Bern
peter.wurz@space.unibe.ch

2021 IEEE Aerospace Conference | 978-1-7281-7436-5/21/$31.00 ©2021 IEEE | DOI: 10.1109/AERO50100.2021.9438344

***Abstract*—The JUpiter ICy moons Explorer (JUICE) of the European Space Agency (ESA) will investigate Jupiter and its icy moons Europa, Ganymede and Callisto, with the aim to better understand the origin and evolution of our Solar System and the emergence of life. The Neutral gas and Ion Mass spectrometer (NIM) is one of six instruments of the Particle Environment Package (PEP) on board the JUICE spacecraft. PEP will measure neutral atoms and molecules, the ion population, and the electron population over an energy range covering from meV to MeV. The NIM instrument is designed to measure the chemical and isotope composition of the exospheres of three of Jupiter's satellites, the icy moons, both, during several flybys and during its final destination in Ganymede orbit. From measurements of the exosphere, we will derive the chemical composition of the surface, which will allow us a better understanding of the icy moons formation processes, interaction processes with the magnetospheric plasma and energetic particles of Jupiter's magnetospheric system.**

The NIM instrument is a compact time-of-flight mass spectrometer allowing measurements of thermal neutral molecules and ionospheric ions. To minimize the background radiation on the detector and protect electronics against the harsh radiation environment around Jupiter, elaborated radiation shielding was designed. NIM consists of two major subunits, namely, the ion-optical system and the electronics.

This study presents details on the technical design and the results obtained from the calibration campaigns of different subsystems of the flight instrument including a mass range of m/z 1 to 650, a mass resolution $m/\Delta m$ of at least 750 (FWHM), and an instantaneous dynamic range of almost 6 decades. These results are discussed in detail with respect to the scientific requirements. This performance in combination with its radiation tolerance allows for both a detailed analysis of the chemical composition of Jupiter's icy moons' exospheres and ionospheres, and to explore environments, where formation of life might be possible.

978-1-7281-7436-5/21/$31.00 ©2021 IEEE

TABLE OF CONTENTS

1. INTRODUCTION

The Neutral gas and Ion Mass spectrometer (NIM) is part of the Particle and Environment Package (PEP) on board the JUpiter ICy moons Explorer (JUICE). JUICE will investigate Jupiter, its radiation environment, and its icy moons Ganymede, Europa and Callisto as potential habitable worlds. The JUICE satellite will launch in June 2022 and will arrive in the Jupiter system in October 2029. It will start with an investigation of Jupiter's atmospheric structure and composition and its fast rotating magnetic field. During this time, JUICE will perform several flybys at Callisto and Ganymede followed up by two flybys at Europa. Europa has a young icy surface with a liquid water ocean beneath touching its silicate mantel. The main objective of the two flybys at Europa is to investigate Europa's non-ice components and its recently active areas, to determine the chemical composition of its exosphere, and its subsurface ocean. After the flybys at Europa, JUICE will use gravity assistance of Callisto to investigate Jupiter's atmosphere at high latitudes. During the flybys at Callisto, JUICE will take measurements of Callisto's internal structure, surface and exosphere. JUICE will then transfer to Ganymede, where it will take a global geological map of Ganymede's surface and investigate the local plasma environment in regards to the interaction of Ganymede's magnetic field with the magnetic field of Jupiter. The nominal mission will end in June 2033 by crashing the spacecraft on Ganymede [1].

PEP, as part of JUICE's scientific payload, consists of six instruments measuring electrons, ions and neutral particles in the energy range of 0.001 eV – 1 MeV to characterize Jupiter's and the moons' plasma environment [2]. NIM will be the first instrument to take in situ measurements of the chemical composition of the icy moons' exospheres. Their exospheres consist of particles released from their surface by ion bombardment, sublimation and photon interaction. With the in situ measurements, we will get a better understanding of the formation processes of the moons' exospheres and surfaces. In addition, we will get information about the surface compositions by the sputtered atoms and molecules.

In this contribution, we provide an overview covering different instrument components such as the ion optical system and the electronics, and present the results obtained on key performance studies such as ion storage capability, sensitivity, and mass resolution of the NIM ion-optical system. All the performance tests presented in this paper were conducted with the laboratory electronics, as the flight electronics was in production.

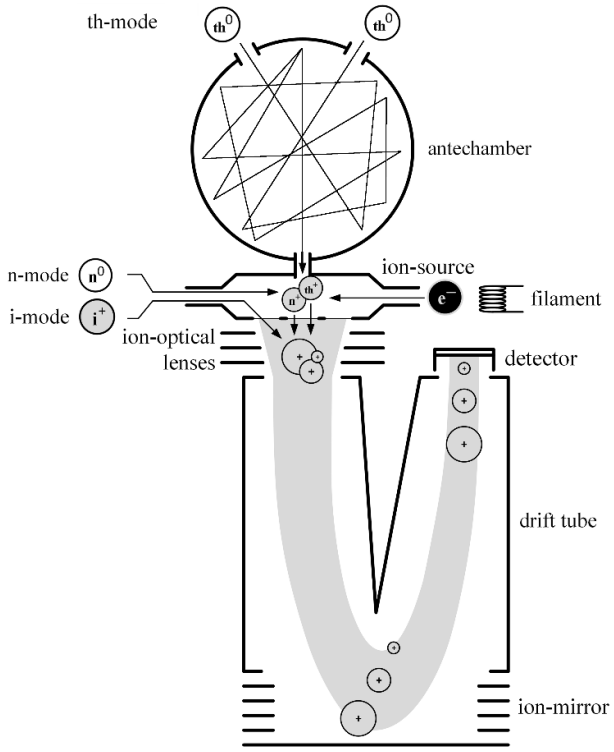

Figure 1. Schematics of the NIM ion-optical system.

Planetary Protection Concept of JUICE

The purpose of planetary protection is to prevent forward contamination of other celestial bodies with terrestrial life forms, and to ensure that future scientific investigations related to the origin of life are not compromised. In addition, it includes a policy for the protection of the Earth from extraterrestrial life carried by a spacecraft from interplanetary sample return missions. There exist five different planetary protection categories for space missions reflecting the level of interest and concern in regards to contamination [3].

The JUICE satellite will perform two flybys at Europa. These flybys are in the Planetary Protection category III because Europa contains a liquid water ocean with a young surface with active areas. JUICE had to demonstrate that the probability of a collision with Europa is below 10^{-4} or had to undergo active bioburden reduction. JUICE will be sterilized by the high radiation flux in the Jupiter system and has therefore not to take any further precautions regarding planetary protection [4].

Ganymede contains, like Europa, a liquid water ocean under a thick ice shell. In contrast to Europa, the liquid water ocean at Ganymede is trapped between two ice layers. The high pressure in the depth generates the lower ice layer [5]. Ganymede has a very old surface (100 million to 2 billion years) and did not show any activity in the recent past although it has some brighter regions where it shows rift valleys and ridges generated by intense surface stresses and

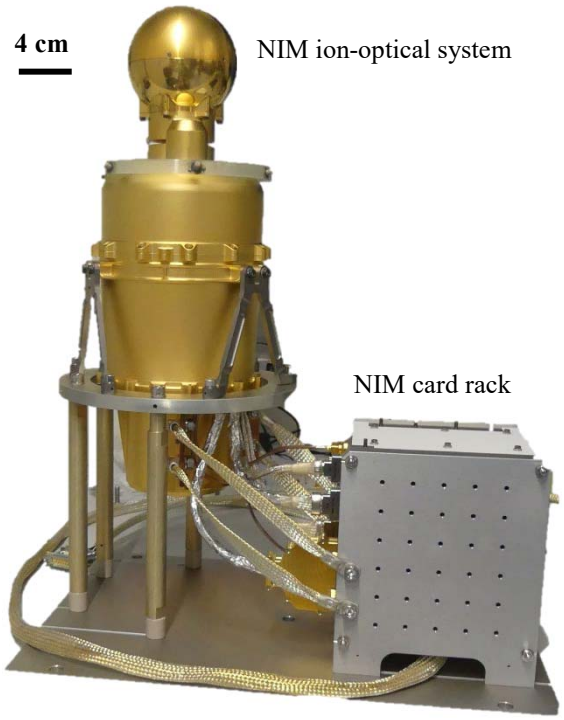

Figure 2. NIM ion-optical system with electronic box (card rack) attached.

subsequent cryovolcanism [6]. JUICE had to show that the likelihood for an organism to reach Ganymede's subsurface ocean is lower than 10^{-4}. The probability of landing in an active region on Ganymede's surface is about $2 \cdot 10^{-3}$. The probability of organisms to survive the cruise phase (10^{-1}), to survive the high radiation dose in Jupiter's orbit (10^{-1}) and the transport on to the surface (10^{-2}), the low probability of the burial mechanism (10^{-4}) reduces all together the total likelihood down to 10^{-11} of a biological contamination on Ganymede's surface. By assuming a typical bioburden of 10^6, which is a nominal value for a standard cleanroom environment, the requirements of 10^{-4} are met by a factor of five [4].

The current flight path of JUICE to Jupiter uses gravity assist of Earth, Mars and Venus. The flyby at Mars is in the Planetary Protection category III and the flyby at Venus is in category II. JUICE showed, that the probability of contamination of these two bodies is below 10^{-2} [4].

2. Design and Methods

NIM is a time-of-flight (TOF) mass spectrometer based on the design of our previous TOF instruments such as RTOF/ROSINA/Rosetta [7, 8], P-BACE/MEAP [9] and NGMS/Luna-Resurs [10, 11]. Compared to other mass spectrometer types, TOF mass spectrometers allow measuring the complete chemical fingerprint of a sample instantaneously instead of scanning over the mass range. This way, a much better spatial resolution during flybys can be obtained, compared to scanning mass spectrometer types such as quadrupole and magnetic sector instruments.

The mass resolution $R = m/\Delta m$ is calculated by $R = t_{tof}/2\Delta t$ where t_{tof} is the time-of-flight of an ion and Δt is the full width at half maximum (FWHM) of the recorded mass signal peak. The longer the drift path is, the longer the drift time t_{tof} will be, which typically results in a better mass resolution. Size limitations of the instrument limit the drift path length. Therefore, NIM uses in addition an ion mirror to almost double the drift path length. Furthermore, the mass resolution is improved by the energy focusing accomplished by the ion mirror [12]. The further possibility to increase the mass resolution would be to reduce Δt by improving the ion-optics for focusing of the ions on the detector.

The signal-to-noise ratio (SNR) is another key parameter in mass spectrometry and is defined as the signal peak height I_{sig} divided by the standard deviation of the noise level I_{noise}: $SNR = I_{sig}/std(I_{noise})$. We designed NIM to measure complex chemical compounds up to masses of 1000 u with a mass resolution up to $m/\Delta m$ 1000 and a SNR exceeding 6 decades [13], although based on present knowledge we do not expect masses higher than 100 u to be observed. The high mass resolution is required to distinguish between different mass peaks at high unit masses. Moreover, for a time-of-flight instrument the SNR is directly proportional to the mass resolution because improvements in the mass resolution are accomplished by improving time focusing and keeping all the ions at the mass line. In the laboratory, we are able to measure the residual gas in the vacuum chamber at a base pressure of a few 10^{-10} mbar. With a SNR of 6 decades, we are able to record partial pressure down to 10^{-16} mbar, which is the detection limit of such an instrument for an integration time of 5 seconds [10]. The highest exospheric pressure from the moons to be measured by NIM during the JUICE mission is in the range of 10^{-8} mbar [14]. NIM's sensitivity is sufficiently high to conduct sensitive chemical measurements at such a low pressure.

The NIM instrument underwent further miniaturization with respect to its predecessor instruments such as NGMS/Luna-Resurs: Whereas the NGMS instrument draws 23 W power in nominal operation [11], NIM will draw 18.5 W of power at maximum. The NIM ion-optical system weighs 3.13 kg where about 48 % of the mass is shielding material of the MCP detector to reduce noise induced by a high flux of energetic electrons accelerated by Jupiter's strong radiation environment. The harsh radiation environment also leads to a special design of the electronics and the detector. The detector has to be very small to minimize the amount of shielding material.

The NIM instrument is divided into two major parts: the ion-optical system and the control electronics (Figure 2). The ion-optical system consists of the actual ion source, the focusing optics, the ion mirror, and the detector (Figure 1). The control electronics consists of five electronic boards hosting low- and high-voltage power supplies, the filament- and motor-controller, the high voltage pulser and two field-programmable gate arrays (FPGAs). The FPGAs control the voltage outputs to the NIM ion-optical system,

they readout and preprocess the detector output signal, and communicate over a data processing unit (DPU) with the spacecraft (S/C).

NIM Ion Optical System

Particle Entrances—NIM allows measurements of neutral atoms and molecules and ionospheric ions. NIM has two entrances: a closed source entrance through an antechamber with a field-of-view (FoV) of 10/3 π sr to thermalize neutral particles, and an open source entrance with a FoV of 300° in azimuth and 10° in elevation angle for neutrals and ions (Figure 1). The antechamber thermalizes incoming neutrals by decelerating them within the interior of the sphere via multiple bounces with the chamber wall. This technique yields also to the particle density enhancement and subsequently an increase of the ion signal intensity while these atoms and molecules pass the ion source [15]. The antechamber's inner surface has to be chemically inert to inhibit chemical alterations of the gases to be measured. This measuring mode is called thermal mode (th-mode). The open source is defined by an entrance slit where neutral particles and ions directly enter the ionization region, without any interaction with the surface structure of the ion source. When measuring with the open source, a shutter closes the flight path between the antechamber and the ion source, to prevent particles collected by the antechamber from entering the ionization region. Incoming neutrals are ionized with an electron-emitting thermionic filament. This measuring mode is called neutral mode (n-mode). When measuring ions the mode is called ion mode (i-mode).

Filaments—NIM uses electron impact ionization with a typical electron energy of approximately 70 eV. Two redundant thermionic emitters provide the electrons in the NIM instrument. We found that BaO and Y_2O_3e filaments are most suitable for our application in NIM with preference to the latter ones [16]. The Y_2O_3e filaments have been designed in cooperation with *Kimball Physics, Wilton, USA*. Compared to the standard Y_2O_3 filaments produced by *Kimball Physics*, the Y_2O_3e filaments used for this application have an increased thickness of the Y_2O_3 coating for increasing their lifetime to 10,000 h operation time. In comparison, the BaO filaments under test have an expected lifetime of about 6,000 h [16]. The heating wires connecting the electron-emitting disc with the filament base of the Y_2O_3e filaments are longer than the wires of the standard Y_2O_3 filaments. Thus, the electron-emitting disc is better thermally decoupled from the filament base, which results in a reduced heat loss, and thus lower power consumption.

Because of the more delicate filament assembly design regarding the mechanical robustness, a few of the filament assemblies of the set of life-time test units were shock- and vibration-tested during the lifetime test for simulation of the transportation to space. The performance of these filaments was compared with the performance of not shocked or vibration tested filaments. Both sets of filaments showed similar performances in terms of power consumption required to reach the target emission and aging behavior. In addition, our life-time tests revealed that the higher temperature needed for Y_2O_3e to emit electrons compared to BaO may have compromised one of the electron beam guiding electrodes (repeller electrode) such that metallic whiskers grew between the repeller electrode and the filament causing a short circuit. Therefore, the material used for the repeller electrode was changed from stainless steel to

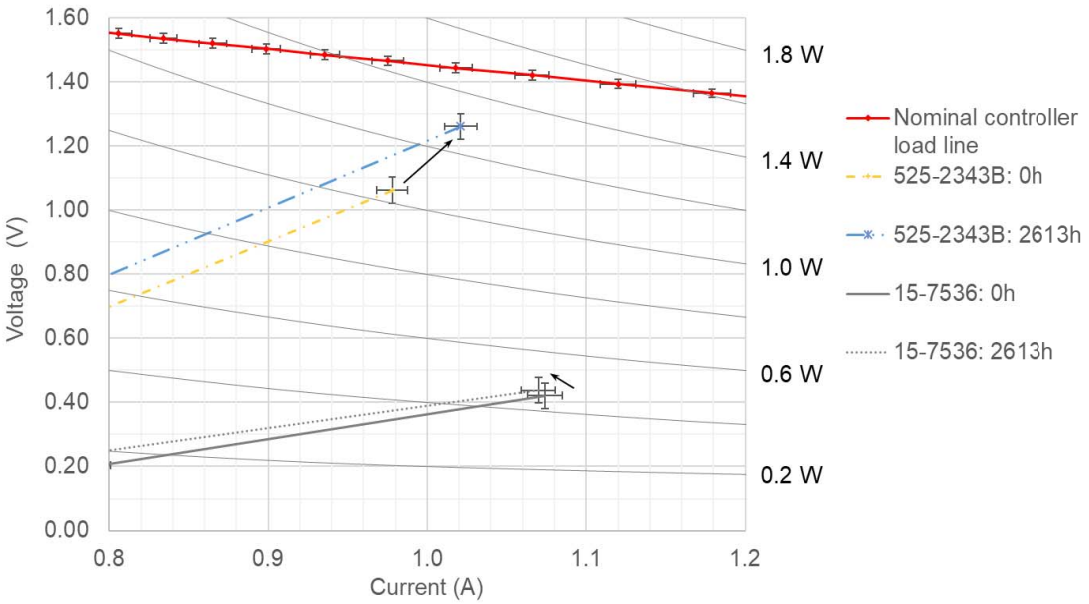

Figure 3. Electrical characteristics of a selected Y_2O_3e (525-2343B) and BaO (15-7536) filament and the Proto Flight filament controller board (Nominal controller load line). The curve for the Proto Flight controller board shows its maximal I-V capabilities at nominal supply voltage of 12.0 V. Hyperbolas in the background show the power levels [16]. Curves for the filaments show the theoretical and measured performance of one BaO and one Y_2O_3e filaments when virgin and after 2613 h of operation.

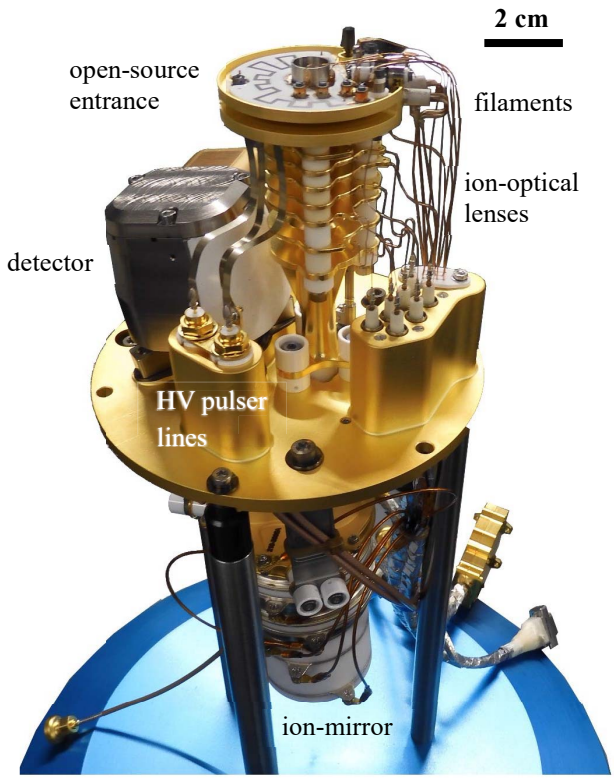

Figure 4. The NIM ion-optical system without the closed-source antechamber.

titanium for the NIM Proto Flight Model (PFM) as titanium is more temperature robust than stainless steel.

Figure 3 summarizes the electrical characteristics of a BaO, an Y_2O_3e filament and the PFM controller board at nominal operation voltage of 12 V DC. The two filaments were operated at a nominal emission current of 50 µA with commercial filament controller boards from *Spacetek Technology AG, Switzerland*. BaO (15-7536) draws less power than Y_2O_3e (525-2343B). The nominal operation time of NIM is about 2,000 h. The power for both filaments can always be provided for both types of filaments.

BaO filaments are known to suffer cathode poisoning when exposed to residual gases such as oxygen [17]. When BaO filaments are exposed to air, a carbonate layer is forming on top of the BaO surface. Therefore, the BaO cathodes have to be activated to get rid of this carbonate layer after every air exposure. The activation procedure is tedious and not favorable for a component used for space instrumentations although this procedure only had to be done once after the spacecraft reaches outer space. However, during calibration and testing in preparation for flight, this is a major complication. Y_2O_3(e) filaments are not affected by residual gas and no complicated conditioning procedure is required after air exposure. Therefore, they are better suited for such applications and the use in laboratory devices.

For the NIM sensor, we decided to use the Y_2O_3e instead of the BaO filaments. Because the Proto Flight filament controller board is able to provide power for the Y_2O_3e filaments, even when they have a higher power consumption than the BaO filaments. The longer lifetime and the simpler conditioning procedure of the Y_2O_3e filaments favor them over the BaO filaments.

Ion Optical System—Produced ions get extracted with a high voltage (HV) pulser creating a pulse with a repetition rate of 10 kHz. An ideal pulse would have a very short fall time of about a ns down from a static voltage bias of the order of volts to the negative extraction high voltage to give all extracted ions the same amount of energy. Ions leaving the ion source before the high voltage pulse is fully applied get less energy resulting in an energy spread and therefore induce a lower mass resolution [18]. Low mass ions have higher velocities at the same energy and leave the ion source faster than high mass ions. Therefore, they are more affected by an insufficiently fast fall time of the extraction pulse than high mass ions.

To allow storage of ions during the time between two extraction pulses, the electrodes in the ion source are kept on very stable potentials. Otherwise, only ions generated during application of the HV extraction pulse pass into the TOF section. Every ion produced but not stored during the time when no extraction pulse is applied, is lost. The ions that are lost onto the drift path produce additional electrical noise by the detector signal and decrease the sensitivity of the instrument [19]. Ion storage is essential for NIM to increase its capabilities while conducting measurements in an environment with pressure limits of 10^{-8} mbar down to 10^{-16} mbar. The ions extracted from the ion source are focused with 7-element ion-optical lenses and fly through the drift tube to the ion-mirror. The ion-mirror is used to increase the flight distance and for energy focusing of the ions.

During the vibration test in November 2019, the ion-source broke due to a bad brazing joint between the last electrode of the ion source and the drift tube, leading to a redesign of the ion-source [20]. In the new design, the electrodes of the ion-source are held together with tree screws with ceramic insulators between the electrodes (Figure 4). A similar design was already used in the NIM prototype.

Detector—The ions are detected with a high-speed Multi-Channel-Plate (MCP) detector. Each ion generates a short current pulse of about 0.5 ns pulse width, inducing a voltage signal of about 5-100 mV on the 50 Ω input of the front-end electronics. This short pulse width requires fast readout electronics with a sample frequency of 2 GHz. The MCP detector has an impedance-matched anode to minimize signal reflections at the cable interfaces [21].

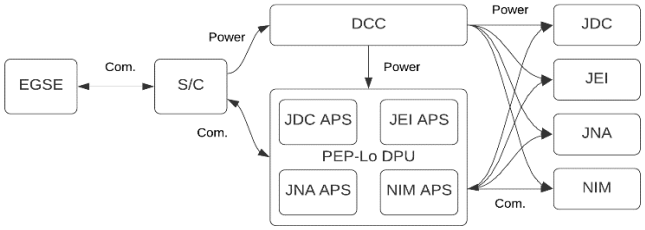

Figure 5. Schematics of the power and communication paths (Com.) between the Electrical Ground Support Equipment (EGSE) and the NIM instrument.

The NIM Electronics

Figure 5 shows a schematic drawing of the communication and power lines from the Electrical Ground Support Equipment (EGSE) to the NIM instrument. Commands from the EGSE are sent to the S/C. The S/C provides power to the DC-DC-Converter (DCC) that provides power for all four instruments indicated in Figure 5. For NIM, the DCC provides five different low voltages. The S/C provides 18.5 W for NIM [13] including 20 % margin. With a power conversion efficiency of the DCC of 72.5 %, the resulting net power consumption of the NIM instrument is 10.7 W. The communication of NIM with the S/C is via a DPU shared with the three other PEP-Lo instruments. The DPU contains hardware interface drivers and builds the interface for the application software (APS) of the different instruments. The APS handles the tele-commands from the spacecraft, prepares and sends the telemetry packages from the different instruments [22]. The DPU communicates over Low Voltage Differential Signaling (LVDS) with NIM. NIM has two FPGAs: a RTSX (Radiation-tolerant Antifuse-based FPGA) and a static random-access memory (SRAM) based Virtex-4.

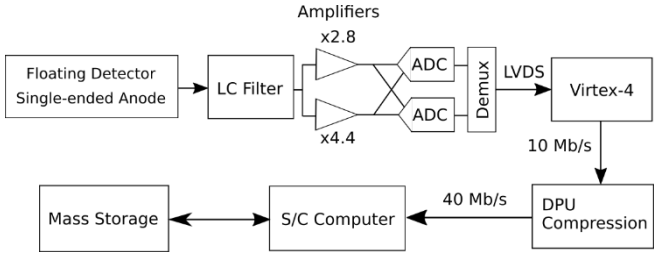

Figure 7. Detector signal path.

To start the NIM instrument, the APS commands the RTSX to load an image of the Virtex-4 from a magnetoresistive random-access memory (MRAM) to the Virtex-4. As soon as the Virtex-4 is started, the RTSX goes into bridge mode, i.e., commands from the DPU addressed to the Virtex-4 pass directly through. The Virtex-4 controls the different low- and high-voltage supplies (see Figure 6) and it is responsible for high-speed data processing by preparing the incoming detector signal. Due to the low on-chip memory capacity (BRAM) of this particular FPGA type, it is important to forward the measured data fast to the DPU for data compression and then further to the S/C mass memory.

Figure 7 shows the signal path of the detector signal. The analog raw signal from the detector is low-pass filtered (antialiasing) and fed into two different amplifiers. Depending on the signals expected amplitude, either the signal from the first or the second amplifier is fed into the two analog-to-digital converters (ADCs). Each ADC has a sampling rate of 1 GS/s resulting in a sampling rate of 2 GS/s when using both ADCs in interleaved mode. The sampled signal is transmitted to the Virtex-4, which generates the actual science data package. It adds information needed to

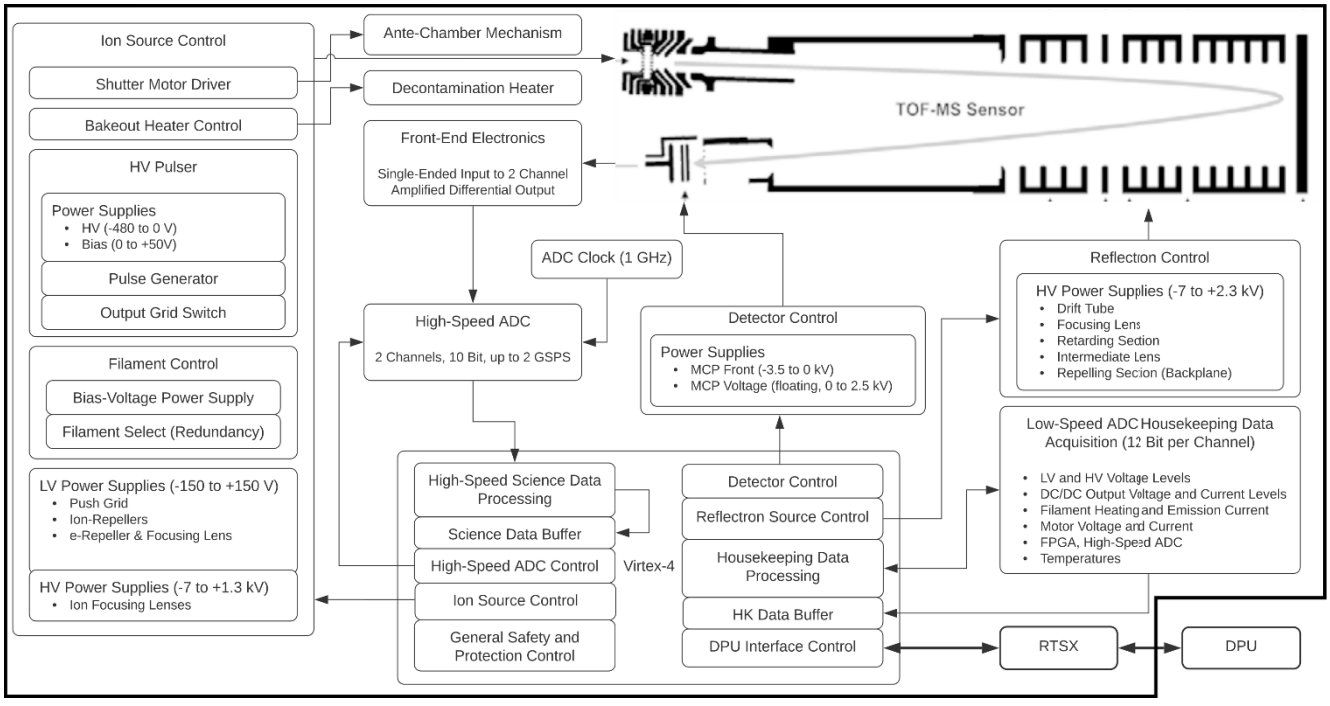

Figure 6. The NIM electronics control schematics.

evaluate the science data such as the emission current of the electron-emitting filament, the used voltage set, data acquisition time, etc., and forwards the data packages to the DPU.

Radiation Protection Concept

Jupiter has a harsh radiation environment mainly consisting of high energetic protons and electrons in the energy range of 0.01 – 50 MeV with a radiation flux of $10^6 – 10^7$ cm^{-2} sr^{-1} s^{-1} MeV^{-1} [23]. Protons are about two orders of magnitude less abundant than electrons and protons are easier to shield because their penetration range in matter is shorter than for electrons. Therefore, we focused the radiation shielding design on shielding against high energetic electrons. This can be done by using dense materials with a high proton number Z to slow down the electrons. These materials have the side effect that the fast electrons produce bremsstrahlung as secondary radiation when decelerated, which has also to be blocked. The production of bremsstrahlung increases with the proton number of the shielding material. For this purpose, we used a tungsten copper alloy as shielding material, which consists of Cu as a low Z material to slow down the electrons and W as high Z material to block the produced bremsstrahlung.

To prevent the NIM electronics from radiation damage, the electronic boards are in a special vault, the card rack, shared with the electronics of other PEP-Lo instruments. The card rack wall consists of 2 mm tungsten copper alloy, keeping the total ionization dose (TID) over the mission of the electronics below 100 kRad including a safety factor of 2 [20]. Components used in electronic circuits were selected by their sufficiently high radiation hardness. The shielding of cables are grounded to inhibit charging. For the FPGAs design we decided to use one radiation hard, one-time programmable (RTSX) and one radiation tolerant, reprogrammable (Virtex-4) FPGA. The radiation mitigation approach for the Virtex-4 follows the following concept: to correct bit flips induced by single event upsets (SEU) caused by the ionizing radiation, the RTSX frequently scrubs the Virtex-4 configuration, i.e. the RTSX overwrites the Virtex-4 configuration SRAM with the image stored in MRAM. In addition, triple-mode redundancy (TMR) and BRAM error correction codes (ECC) are implemented for the most critical functions executed by the Virtex-4, such as control loops for high-voltage cascades and filament current, safety limit checks, etc.

The most critical part in the ion-optical system is the MCP detector. High energetic electrons and ions increase the noise background, which leads to a lower sensitivity of the instrument. Without shielding, the count rate is about 10^5 counts/sec resulting in 10 counts per single waveform in Europa's radiation environment. To reduce the shielding volume of the detector, we used a flex printed circuit board (PCB) to fold the detector proximity electronics inside a small volume. Extensive simulations were done to get the optimal shielding design. The design was tested at the *High Intensity Proton Accelerator Facility, PSI Villigen, Switzerland* [24, 25, 26]. The detector shielding consists of an aluminum housing of 1 mm thickness covered by a 10 mm tungsten copper shielding. The outer shell of the NIM ion-optical system consists of 1 mm AlBeMet, a material consisting of aluminum and beryllium. In addition, a 6 mm tungsten copper shielding disc array is positioned behind the ion-mirror opposite the detector entrance to shield against radiation entering the detector directly. With this shielding concept, the noise level induced by radiation could be reduced by a factor of 100 [26].

As we verified the radiation shielding design of the detector, no further tests with the actual PFM detector are planned [24, 25, 26]. Radiation tests with the flight hardware would expose the flight hardware and detector to a siginifcant radiation dose before launch. Most likely, the sensor would have to remain a the radiation facility until the detector material activated during the test is no longer radioactive. This would be incompatible with the current schedule because the PFM sensor was delivered for integration onto the spacecraft in December 2020.

Measurement Conditions

All measurements were performed in a vacuum chamber with a chamber pressure of $1 \cdot 10^{-8}$ mbar or lower. The tests were done in the CASYMIR test facility located at the University of Bern [27]. CASYMIR is able to generate a neutral gas beam with velocities up to 5.5 km/s by heating the gas to a temperature of 600°C. The average beam velocity depends on the gas temperature and the mean molecular mass of the gas. To reach higher beam velocities, the amount of the carrier gas H_2 relative to the test gas has to be increased. CASYMIR has a gas inlet system to inject gases directly into the chamber with a leak valve to increase the chamber pressure with the test gas. For measurements where a neutral gas beam was used, the beam consisted of H_2 and Kr with a ratio of 20:1 unless otherwise mentioned. The chosen beam velocity was 2 km/s because that is the velocity of the S/C in Ganymede orbit, which will be 90% of the measuring time of the NIM instrument. All measurements were performed with the NIM PFM ion-optical system with the laboratory electronics attached.

3. Results and Discussion

In this chapter, we discuss different performance tests of the NIM PFM ion-optical system. We also discuss the ion storage capability of the ion source subsequently followed by performance results of the ion optical system ($m/\Delta m$, SNR, mass range).

Ion Storage Capability

Ion storage during the time between two extraction pulses is essential to increase the sensitivity of the NIM instrument. Ion storage is facilitated by properly shaping the electron beam used for ionization [19]. We tested the ion storage capability for th-mode and n-mode of the ion-optical system with a neutral gas beam. The chamber pressure was

$(2 – 5) \cdot 10^{-9}$ mbar. The electron emission current I_{em} was varied in the range from 40 – 400 µA. When changing the electron emission current, the electric potential distribution in the ion source changes. Therefore, we optimized the low voltage electrodes in the ion source for each data point. Especially the backplane electrode opposite to the ion extraction grid changed significantly between 0 and –3.8 V depending on the voltage set and the electron emission current. In Figure 9, the corresponding electrode was set to -1.7 V. To focus the electron beam, this electrode had to be set to a more negative voltage the higher the electron emission current was applied. The electron beam holds the ions in the two spatial dimensions orthogonal to the electron propagation. In the dimension of the electron flight path, the ions are kept by the electric field generated by the low-voltage electrodes. These electrodes are in our source at around 130 ± 20 V depending on the electron emission current. They generate a strong positive field ring in the plane of the ion extraction grid and trap the ions in the direction of the electron flight path. Figure 9 shows the electric field with a sample voltage set of the ion source.

Figure 8 shows the measured data for the collected ion signal as a function of electron emission current. The data were fitted with a linear function for data points between 0 and 100 µA and with a quadratic function for emission currents higher than 100 µA. Kr was part of the neutral gas beam and H_2O was part of the residual gas inside the vacuum chamber. Up to 100 µA, the signal increases linearly with the emission current proportionally to the increase in electron current, and no ions are stored for I_{em} below 100 µA. Above 100 µA emission current, the signal intensity increases with a power law I_{em}^n with n between 2 and 3. Thus, the ion source shows an ion storage capability for all gases. When the emission current is increased from nominal 100 µA to 300 µA, we gain a factor of 3 in signal intensity directly from the current increase. Due to the ion storage capability, we gain an additional factor of 4 resulting in 12 times higher

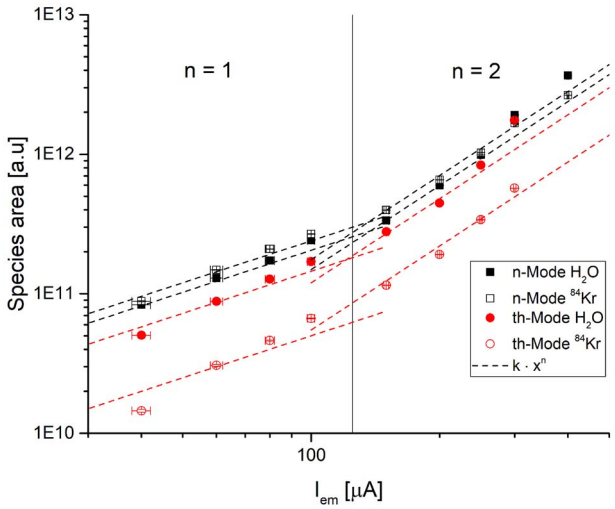

Figure 8. Ion storage capability of the NIM instrument for n-mode and th-mode. A neutral gas beam consisting of H_2 and Kr was used. H_2O was part of the residual gas.

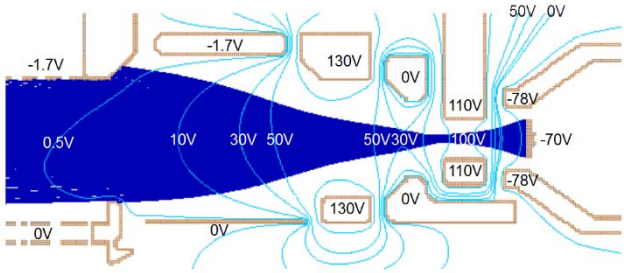

Figure 9. Ion source with sample voltage set applied the electrodes. In light blue are the potential lines and in dark blue simulated electron beam.

signal intensity when increasing the emission current by a factor of 3 as a proposed high sensitivity mode.

Ion storage is expected in the th-mode only, because the neutral atoms and molecules enter the ionization region perpendicular to the electron beam at thermal energies. The NIM instrument has a specially designed ion-source to store ions also in the n-mode. The generated ions in the n-mode have an initial velocity along the direction of the electron beam. The particular configuration of the ion repelling ring electrodes serves for the latter confinement of the ions produced inside this potential ring (electrodes with voltage +130 V in Figure 9). Atoms and molecules entering the ion-source with a velocity between 1 and 8 km/s and a mass between 1 and 100 u have a maximum kinetic energy of 33 eV and are easily trapped in this field configuration. For the Europa flyby where the S/C velocity is 4 km/s, masses up to 1000 u reach a kinetic energy of 80 eV and are therefore trapped in the potential field. The electric field also widens and defocuses the electron beam. Simulations with the software *SIMION from Scientific Instrument Services Inc. version 8.1.3* show, that the applied electric field focuses the electron beam (Figure 9) and makes ion storage possible also for ions entering the ion source in the direction of the electron flight path as it is observed in the n-mode.

Density enhancement behavior of the antechamber

Atoms and molecules enter the ionization region either directly through the open source entrance or they enter first the antechamber, where they get thermalized before they enter the ionization region. The total number density n_{tot} in the ionization region is the sum of particles entering the ionization region through the closed source entrance n_{cs} and particles entering the ionization region directly via the open source n_{os}. With the test facility, we are only able to direct the neutral gas beam through one of the two entrances at a time. Therefore, the total number density in the ionization region is equal to the contribution of the closed source. n_{cs} is then:

$$n_{cs} = n_a \sqrt{\frac{T_a}{T_s}} \frac{F(S)\, k\, \sin^2(\omega/2)\, \cos^2(\omega/2)}{1 - k \cos^2(\omega/2)} \frac{d_i^2}{d_i^2 + d_s^2} \qquad (1)$$

$$F(S) = e^{-S^2} + \pi^{1/2}\, S\, (1 + \mathrm{erf}(S))$$

$$S = v_{sc} \cos\chi \sqrt{\frac{m}{2k_B T_a}}$$

Where n_a is the number density of the neutral gas beam, T_a is the ambient gas temperature corresponding to the temperature of the neutral beam. T_s is the ion source temperature, k is the probability of a molecule being re-emitted after colliding with the surface. $k \approx 1$ for the gases we used for calibration. ω is the cone half-angle of the open source, d_i the opening diameter of the antechamber, d_s the diameter of the exit hole to the ion source. v_{sc} is the spacecraft velocity corresponding to velocity of neutral gas beam, χ the angle of the spacecraft with respect to the surface normal of the entrance aperture, m the mean molecular mass of the gas beam and k_B the Boltzmann-constant. With increasing spacecraft velocity v_{sc}, the number density in the ionization region has to increase when measuring with the closed entrance [28, 15].

To test this behavior, the neutral particle intensity was measured for different beam velocities. The beam velocity was varied by changing the mass ratio of H_2 to Kr in the neutral gas beam. This corresponds to a variation of the mean molecular mass of the beam and therefore to a variation in the beam velocity. The data in Figure 10 are pressure and flux corrected to take into account the decreasing signal intensity of Kr with increasing beam velocity due to the lower amount of Kr in the beam compared to H_2.

The measured data follow nicely the theoretical model for the two test gases. With H_2 and Kr we covered the main mass range of interest because Kr has a mass of 84 u. Earlier tests showed that the isotopic ratio of molecules measured with the antechamber are similar to the fragmentation pattern measured when molecules enter via the open source [28]. This indicates that no additional fragmentation happens in the antechamber due to collisions and chemical interactions of the molecules with the antechamber inner walls. Therefore, we successfully verified the proper functionality of the antechamber.

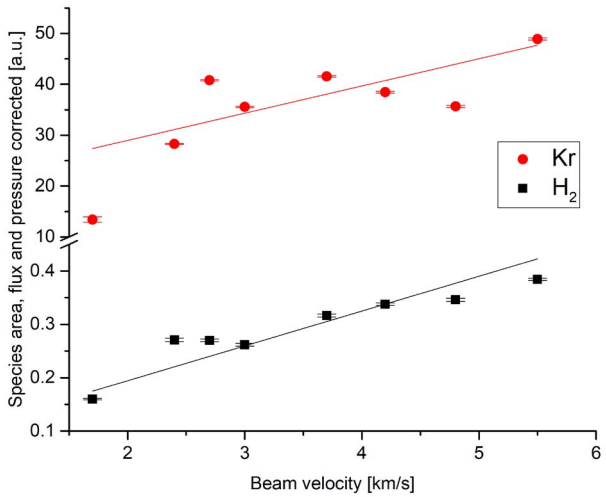

Figure 10. Signal intensity measured with the closed source antechamber in dependence of the velocity with H_2 and Kr as test gases.

Mass Range

NIM is supposed to measure masses up to 1000 u [4]. In the moons' exospheres, we only expect masses up to 100 u, unless something completely unexpected is present. However, with the ability to measure up to higher mass ranges, we will be able to measure also potential organic compounds with high masses up to 1000 u [29]. The calibration gas perfluoropheneanthrene (CAS nr. 306-91-2, chemical formula $C_{14}F_{24}$) was used to verify the performance of NIM to measure heavy species. Perfluoropheneanthrene breaks up into many fragments with different unit mass up to 624 u, the parent mass, when ionized with an electron beam, making it a common calibration substance for TOF mass spectrometers. The liquid test substance was heated to bring it into the gas phase. The gas was injected into the chamber with a leak valve set so that the chamber pressure increased to $6.6 \cdot 10^{-8}$ mbar. The filament emission current was set to 420 µA and the MCP voltage was set to 1.9 kV. Figure 11 shows the recorded mass spectrum, featuring mass peaks over the entire spectrum range. The mass with the lowest signal intensity tabulated by the manufacturer is mass 624 u, which is clearly visible in our mass spectrum. We even see a clear mass peak at 642 u, which is not tabulated by the manufacturer but results from a water adduct to the parent molecule.

Mass Resolution

According to the requirements stated in [20], NIM has to reach a mass resolution $m/\Delta m$ of 500 but to distinguish between different species of masses up to 1000 u, a mass resolution of 1000 is required. In addition, the previously built instrument at our institute, the NGMS instrument from

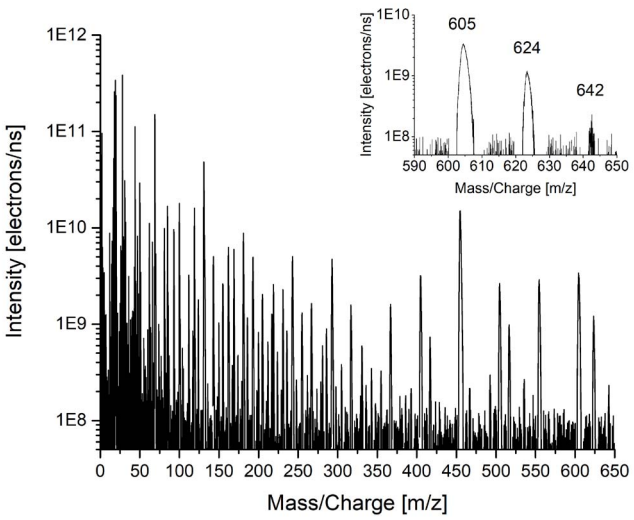

Figure 11. Mass spectrum recorded with NIM with FC5311 as calibration gas. Tabulated masses are up to 624 u. Highest mass recorded is 642 u. Chamber pressure was $6.6 \cdot 10^{-8}$ mbar. The filament emission current was 420 µA the MCP voltage was 1.9 kV.

the Luna-Resurs mission, reaches a mass resolution of 1000 [11]. Our aim for the NIM instrument is to achieve the same or a better performance than NGMS. Figure 12, left panel, shows a mass spectrum measured with the th-mode and Figure 12, right panel, shows a mass spectrum recorded with the n-mode. We used a neutral gas beam consisting of H_2 and Kr. The electron emission current for the th-mode was 60 µA and 100 µA for the n-mode. The mass spectra were recorded during the ion storage calibration campaign.

The peaks at *m/z* 85 and 87 are artifacts generated by the readout electronics. These peaks appear after mass peaks with a high signal intensity and start with a down slope before reaching their maximum. The ^{78}Kr isotope is barely above the noise level in the mass spectra due to the low electron emission current used for both measurements (see Figure 12). The Kr mass peaks appear slightly below their integer mass number due to the preliminary mass calibration. The peak shapes of the ^{78}Kr peaks are similar to the peak shape of the other Kr peaks. The small peak at m/z 78.66 in the th-mode spectrum could only be a triply charged species. In this case, also the single and double charged peaks of that species have to be visible because they are easier to detect, which is not the case. Therefore, we can conclude that this peak is a noise peak. The peak at m/z 79 is most likely noise.

The mass resolution for ^{84}Kr in the th-mode is $m/\Delta m$ 757 (FWHM) and the mass resolution in the n-mode is $m/\Delta m$ 534 (FWHM). The mass resolution in the n-mode is readily lower than the mass resolution measured in the th-mode because the incoming particles have a significant initial kinetic energy and they have to be deflected by 90° in the ion source to pass them into the drift tube. In the th-mode particles enter the ion-source straight and are therefore easier to accommodate and focus towards the detector system. Both modes fulfill the mission science requirements by having a mass resolution $m/\Delta m$ higher than 500 but the mass resolution is smaller than the mass resolution we want to achieve. With the actual flight electronics, we expect to reach a higher mass resolution.

There is an additional aspect of the mass resolution in relation to the signal-to-noise ratio (SNR). In a TOF mass

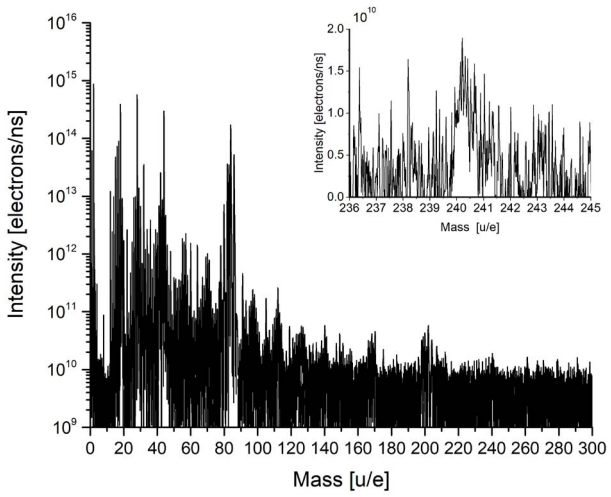

Figure 13. Mass spectrum recorded with NIM's th-mode showing a SNR of almost 6 decades.

spectrometer, the mass resolution is established by focusing the ion packets in time and not by reducing the phase space of the ions like in other mass spectrometers (e.g. sector magnet instruments). Thus, for a higher mass resolution the peaks become higher and narrower which directly improves the SNR. Moreover, since the peaks become narrower, the contribution by noise becomes less since fewer time bins in the TOF spectrum are affected, which adds to the improvement in SNR. In summary, even if the high mass resolution is not needed for the spectral separation of species, every improvement in mass resolution improves the SNR in a TOF mass spectrometer.

Signal-to-Noise Ratio

The expected particle density of Europa's exosphere at a height up to 10'000 km above the moon's surface is in the range of 10 – 10^8 cm^{-3} [14], which corresponds to a pressure of 10^{-15} – 10^{-8} mbar. The closest distance the S/C will have to the moon's surface will be 400 km [30]. To conduct optimal measurements of Europa's exosphere, NIM has to achieve a SNR of about six decades. The tests were performed at a pressure of 10^{-9} mbar. The electron emission current was set

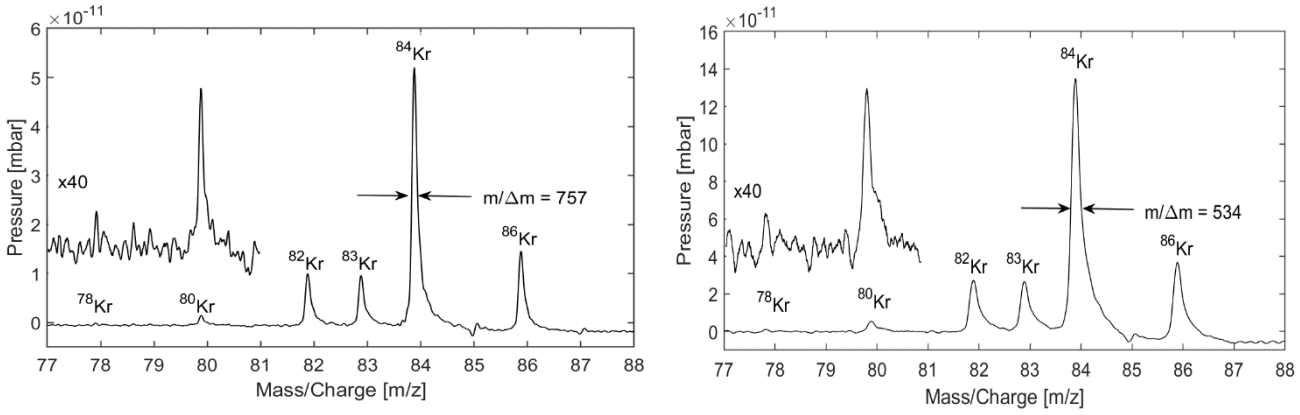

Figure 12. Two mass spectra recorded using NIM with a neutral gas beam consisting of H_2 and Kr with a ratio of 20:1. Left: Kr recorded in th-mode. The electron emission current was 60 µA. Right: Kr recorded in n-mode. The electron emission current was 100 µA.

to 400 µA in this study and we measured with a neutral gas beam. Figure 13 demonstrates the maximum SNR we were able to measure until now with the NIM ion-optical system. In the th-mode NIM reaches a SNR of almost 6 decades comparing the hydrogen peak and the peak at mass 240 u. This peak is a hydrocarbon peak originated from the residual gas compounds present in the vacuum chamber.

The SNR and the mass resolution depend on the proper focusing of the ions on the detector. The areas under the mass signal peaks are proportional to the number of detected ions of the corresponding mass peak. A better focusing of the ions on the detector leads to narrower and higher mass peaks because the area under the peaks stays the same. Therefore, a better focusing of the ions improves both the mass resolution and the SNR. The NIM ion-optical system has 19 focusing electrodes to be optimized and laboratory tests are still under investigation to improve the voltage set to reach higher performance.

4. SUMMARY

We introduced the NIM instrument electric structure and functionality including its connection to the spacecraft. We presented also the measurement results obtained with the NIM flight ion-optical system with laboratory electronics attached. We demonstrated a mass range of 642 u and a mass resolution of $m/\Delta m$ 750 (FWHM) for the th-mode and of $m/\Delta m$ 530 (FWHM) for the n-mode. NIM has a dynamic range of almost 6 decades and a good ion storage capacity.

NIM fulfills the requirements regarding mass resolution and dynamic range, although there the instrument will be further optimized during the cruise phase when optimizing the voltage sets applied to the electrodes of the ion optical system. The PFM was delivered for integration onto the JUICE spacecraft in December 2020. In early January 2021, the first tests of the whole instrument with flight electronics attached will start. These tests will be performed with the flight spare model.

ACKNOWLEDGMENTS

This project is supported by the Swiss Space Office through the ESA PRODEX program and by the Swiss National Science Foundation. The authors would like to thank also the many contributors at the University of Bern. Special thanks are to H.R. Elsener of EMPA for the invaluable collaboration. Moreover, we acknowledge the support of the PEP team, in particular: S. Karlsson (IRF), S. Jaskulek (JHU/APL), and S. Barabash (IRF).

REFERENCES

[1] O. Grasset, M. K. Dougherty, A. Coustenis, E. J. Bunce, C. Erd, D. Titov, M. Blanc, A. Coates, P. Drossart, L. N. Fletcher, H. Hussmann, R. Jaumann, N. Krupp, J.-P. Lebreton, O. Prieto-Ballesteros, P. Tortora, F. Tosi and T. Van Hoolst, "JUpiter ICy moons Explorer (JUICE): An ESA mission to orbit Ganymede and to characterise the Jupiter system," *Planetary and Space Science,* vol. 78, pp. 1-21, 2013.

[2] S. Barabash, S. Karlsson, M. Wieser, P. Brandt, J. Westlake, P. Wurz and M. Fränz, "Radiation mitigation in the Particle Environment Package (PEP) sensors for the JUICE mission," *European Planetary Science Congress,* vol. 10, 2015.

[3] COSPAR, "COSPAR Policy on Planetary Protection," 17 June 2020.

[4] H. Hussmann, P. Palumbo, R. Jaumann, M. Dougherty, Y. Langevin, G. Piccioni, S. Barabash, P. Wurz, P. Brandt, L. Gurvits, L. Bruzzone, J. Plaut, J.-E. Wahlund, B. Cecconi, P. Hartogh, R. Gladstone, L. Iess, D. J. Stevenson and Y. Kaspi, JUICE JUpiter ICy moons Explorer Exploring the emergence of habitable worlds around gas giants around gas giants, European Space Agency, 2014.

[5] O. Grasset, E. Bunce, A. Coustenis, M. K. Dougherty, C. Erd, H. Hussmann, R. Jaumann and O. Prieto-Ballesteros, "Review of Exchange Processes on Ganymede in View of Its Planetary Protection Categorization," *Astrobiology,* vol. 13, pp. 991-1004, 2013.

[6] G. Collins und T. V. Johnson, «Chapter 37 - Ganymede and Callisto,» in *Encyclopedia of the Solar System (Third Edition)*, Elsevier, 2014, pp. 813 - 829.

[7] H. Balsiger, K. Altewg, P. Bochsler, P. Eberhardt, J. Fischer, S. Graf, A. Jäckel, E. Kopp, U. Langer, M. Mildner, J. Müller, T. Riesen, M. Rubin, S. Scherer, P. Wurz, S. Wüthrich and E. Arjis, "Rosina – Rosetta Orbiter Spectrometer for Ion and Neutral Analysis," *Space Science Reviews,* vol. 128, pp. 745-801, 2007.

[8] S. Scherer, K. Altweg, H. Balsiger, J. Fischer, A. Jäckel, A. Korth, M. Mildner, D. Piazza, H. Reme und P. Wurz, «A novel principle for an ion mirror design in time-of-flight mass spectrometry,» *International Journal of Mass Spectrometry,* Bd. 251, pp. 73-81, 2006.

[9] D. Abplanalp, P. Wurz, L. Huber, I. Leya, E. Kopp, U. Rohner, M. Wieser, L. Kalla and S. Barabash, "A neutral gas mass spectrometer to measure the chemical composition of the stratosphere," *Advances in Space Research,* vol. 44, no. 7, pp. 870-878, 2009.

[10] P. Wurz, D. Abplanalp, M. Tulej and H. Lammer, "A neutral gas mass spectrometer for the investigation of lunar volatiles," *Planetary and Space Science,* vol. 74,

no. 1, pp. 264-269, 2012.

[11] R. G. Fausch, P. Wurz, M. Tulej, J. Jost, P. Gubler, M. Gruber, D. Lasi, C. Zimmermann and T. Gerber, "Flight electronics of GC-mass spectrometer for investigation of volatiles in the lunar regolith," *2018 IEEE Aerospace Conference,* pp. 1-13, 2018.

[12] B. A. Mamyrin, V. I. Karataev, D. V. Shmikk and V. A. Zagulin, "The mass-reflectron, a new nonmagnetic time-of-flight mass spectrometer with high resolution," *Zh. Eksp. Teor. Fiz.,* vol. 64, pp. 82-89, 1973.

[13] H. Andersson, P. Wurz, P. Brandt, S. Jaskulek and S. Barabash, "PEP EID- B (SE-01)," University of Bern, Bern, 2020.

[14] A. Vorburger and P. Wurz, "Europa's Ice-Related Atmosphere: The Sputter Contribution," *Icarus,* vol. 311, 2018.

[15] P. Wurz, A. Balogh, V. Coffey, B. K. Dichter, W. T. Kasprzak, A. J. Lazarus, W. Lennartsson and J. P. McFadden, "Calibration Techniques," ISSI Scientific Report Series, 2007.

[16] R. G. Fausch, "Mass Spectrometry for In Situ Planetary Research," University of Bern, Bern, 2020.

[17] H. Friedenstein, S. L. Martin and G. L. Munday, "The mechanism of the thermionic emission from oxide coated cathodes," *Reports on Progress in Physics,* vol. 11, no. 1, pp. 298--341, 1947.

[18] P. Wurz, *Lecture Notes Mass Spectrometry and Ion Optics,* Bern, 2017.

[19] D. Abplanalp, P. Wurz, L. Huber and I. Leya, "An optimised compact electron impact ion storage source for a time-of-flight mass spectrometer," *International Journal of Mass Spectrometry,* vol. 294, no. 1, pp. 33-39, 2010.

[20] D. Lasi, S. Meyer, D. Piazza, M. Lüthi, A. Nentwig, M. Gruber, S. Brüngger, M. Gerber, S. Braccini, M. Tulej, M. Föhn and P. Wurz, "Decisions and Trade-Offs in the Design of a Mass Spectrometer for Jupiter's Icy Moons," *2020 IEEE Aerospace Conference,* pp. 1-20, 2020.

[21] P. Wurz and L. Gubler, "Impedance-matching anode for fast timing signals," *Review of Scientific Instruments,* vol. 65, no. 4, pp. 871-876, 1994.

[22] M. Gruber, P. Gubler, M. Lüthi, P. Wurz and D. Lasi, "PEP-Lo NIM Instrument SW Design Document (ISDD)," 2017.

[23] H. D. Evans, E. J. Daly, P. Nieminen, G. Santin and C. Erd, "Jovian Radiation Belt Models, Uncertainties and Margins," *IEEE Transactions on Nuclear Science,* vol. 80, no. 4, pp. 2397-2403, 2013.

[24] H. Wojtek, L. Desorgher, K. Deiters, D. Reggiani, T. Rauber, M. Tulej, P. Wurz, M. Luethi, K. Wojczuk and P. Kalaczynski, "High Energy Electron Radiation Exposure Facility at PSI," *Journal of Applied Mathematics and Physics,* vol. 2, pp. 910-917, 2014.

[25] M. Tulej, S. Meyer, M. Lüthi, D. Lasi, A. Galli, D. Piazza, L. Desorgher, D. Reggiani, W. Hajdas, S. Karlsson, L. Kalla and P. Wurz, "Experimental investigation of the radiation shielding efficiency of a MCP detector in the radiation environment near Jupiter's moon Europa," *Nuclear Instruments and Methods in Physics Research Section B Beam Interactions with Materials and Atoms,* vol. 383, pp. 21-37, 2016.

[26] D. Lasi, M. Tulej, S. Meyer, M. Lüthi, A. Galli, D. Piazza, P. Wurz, D. Reggiani, H. Xiao, R. Marcinkowski, W. Hajdas, A. Cervelli, S. Karlsson, T. Knight, M. Grande and S. Barabash, "Shielding an MCP Detector for a Space-Borne Mass Spectrometer Against the Harsh Radiation Environment in Jupiter's Magnetosphere," *IEEE Transactions on Nuclear Science,* vol. 54, no. 1, pp. 605-613, 2017.

[27] S. Graf, K. Altweg, H. Balsiger, A. Jäckel, E. Kopp, U. Langer, W. Luithardt, C. B. Westermann and P. Wurz, "A cometary neutral gas simulator for gas dynamic sensor and mass spectrometer calibration : Space simulations in laboratory: Experiments, instrumentation, and modeling," *Journal of Geophysical Research,* vol. 109, 2004.

[28] S. Meyer, M. Tulej and P. Wurz, "Mass spectrometry of planetary exospheres at high relative velocity: direct comparison of open- and closed source measurements," *Geoscientific Instrumentation, Methods and Data Systems Discussions,* pp. 1-2, 08 2016.

[29] P. Wurz, D. Lasi, N. Thomas, D. Piazza, A. Galli, M. Jutzi, S. Barabash, M. Wieser, W. Magnes, H. Lammer, U. Auster, L. Gurvits and W. Hajdas, "An Impacting Descent Probe for Europa and the Other Galilean Moons of Jupiter," *Earth, Moon, and Planets,* 2017.

[30] S. Meyer, Development of a Neutral Gas- and Ion-Mass Spectrometer for Jupiter's Moons, Bern: University of Bern, 2017.

BIOGRAPHY

Martina Föhn *received an M. Sc. In physics from the University of Bern in 2017, with a thesis on the scattering properties of charge state conversion surfaces for space applications for the JUICE and the IMAP missions. She is now pursuing a Ph.D. in physics and is responsible for the calibration of NIM.*

André Galli *received a Ph.D. in Physics from the University of Bern in 2008. After a period as an engineer and technology consultant and his post-doctoral period at the Netherlands Institute for Space Research, he re-joined in 2012 the University of Bern as a scientist. His research topics cover a broad range from laboratory experiments in the context of icy surfaces in the solar system, data analysis for space missions (Mars Express, Venus Express, IBEX, Rosetta), to project science and management for upcoming space missions (JUICE and IMAP in particular).*

Audrey Vorburger *holds a B.S. and a M.Sc. in Electrical Engineering and Information Technology that she obtained from ETH Zurich in 2008. In 2013 she received her Ph.D. in Physics from the University of Bern. Having spent one and a half years as a post-doctoral researcher the American Museum of Natural History in NY, USA, she is now back at the University of Bern perusing her teaching certificate. She is a Co-I of SARA onboard Chandrayaan-1 and of PEP onboard JUICE.*

Marek Tulej *received a Ph.D. in Physical Chemistry from the University of Basel in 1999. After his post-doctoral period at Paul Scherrer Institute, he joined in 2008 the University of Bern as an instrument scientist for space missions, including Phobos-Grunt, Marco Polo-R, Luna-Resurs, and JUICE.*

Davide Lasi *received a B.Sc. and an M.Sc. in Chemistry from the University of Milano in 2004 and 2006, and an M.S. from MIT in 2018 (System Design and Management). He has been with the University of Bern since 2011, as project manager for the development of three space mass spectrometers, including NIM for JUICE. Since 2020, he is with the Thirty Meter Telescope (TMT).*

Andreas Riedo *received his Ph.D. in Physics in 2014 from the University of Bern. In 2016 he received a SNSF fellowship that allowed him to continue his research in Astrobiology at the Leiden University, The Netherlands. He extended his stay at the Leiden University with a MCSA fellowship for another two years before he moved in 2019 to the Free University Berlin after receiving the prestigious Einstein fellowship. In 2020 he moved to University of Bern and is currently appointed as researcher and project manager within the JUICE space mission.*

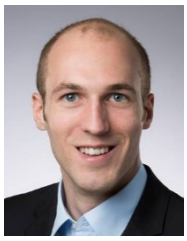

Rico Fausch *completed an apprenticeship as technical designer before he received a B.Sc. in Systems Engineering (micro technologies) from NTB University of Applied Science (Switzerland) in 2013 and a M.Sc. in Biomedical Engineering from University of Bern (Switzerland) in 2015. He has been with the Physics Institute of the University of Bern since 2016, where he received his Ph.D. in Physics in 2020 for the finalization of the NGMS/Luna-Resurs. As a post-doctoral researcher, he is involved in the design of several missions and space instrumentation including NIM/JUICE.*

Michael Althaus *received a HTL & B.Sc. in Electrical Engineering from Lucerne University of Applied Sciences and Arts with specialization in Information Technology in 1999. He worked as a research engineer at ESEC SA in Switzerland and at the Centre for Advanced Materials Joining, University of Waterloo, Canada. Before joining the University of Bern in 2018 for the NIM (JUICE) and the NGMS (Luna-Resurs) instruments, he worked as an R&D SW/HW engineer in the industry.*

Stefan Brüngger *received a B.Sc. in Mechanical Engineering from Bern University of Applied Sciences in 2007 and a M.Sc. in Systems Engineering Management from University College London in 2020. He joined the University of Bern in 2011 as mechanical development engineer. Since then he has worked on the design, development, integration and test of time of flight mass spectrometers and laboratory instrumentation, encompassing NIM for the ESA mission JUICE.*

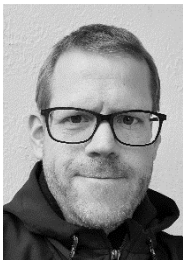

Philipp Fahrer *received a B.Sc. in Electrical Engineering from Bern University of Applied Sciences in 2002. Before he joined the University of Bern in 2018, he worked as a hardware and FPGA design engineer in the industry.*

Michael Gerber *has been employed as a systems engineer at the University of Bern since 2014, where he works on ExoMars Cassis and JUICE PEP. He graduated in mechanical engineering in 2006 and moved to the University of Bern from RUAG Aviation where he was a systems engineer on fighter aircraft.*

Matthias Lüthi *holds an M.Sc. from ETH, Zürich (1996) and an EMBA in management of technology from EPF Lausanne (2009). He has more than 20 years of experience as a hardware design engineer and manager in high-tech industries in the US and Switzerland. He is the NIM electronics systems engineer.*

Hans Peter Munz *received a B.Sc. in Engineering from Bern University of Applied Sciences in 1994. He worked as Software Engineer for Swiss companies for more than 20 years. In 2018 he joined NIM team in this function.*

Severin Oeschger *received a B.Sc. in Microelectronics & Sensors from the Northwest University of Applied Sciences FHNW (Switzerland) in 2007. He is experienced in Electronics and Sensors as Electrical Engineer in research and development for more than 15 years. After working for a Swiss hearing aid brand, he joined the electronic group within the Space Research & Planetary Science Division in 2014. Where he worked as electrical engineer for the CHEOPS mission. He is currently working on the analogue hardware of the Neutral and Ion Mass Spectrometer (NIM) part of PEP on board ESA mission JUICE.*

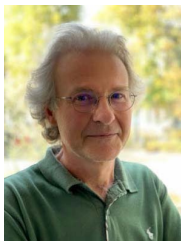

Daniele Piazza *has more than 20 years of experience in the design and development of space instruments. He has a Ph.D. in mechanical engineering from ETH Zurich and started his career in Formula 1. Since 2005 he leads the mechanical engineering group working on space instruments at the University of Bern.*

Peter Wurz *has a degree in electronic engineering (1985), an M.Sc. and a Ph.D. in Physics from Technical University of Vienna (1990). He has been a post-doctoral researcher at Argonne National Laboratory. At the University of Bern since 1992, he is a Professor of physics and since 2015 head of the Space Science and Planetology division. He has been Co-I and PI for many science instruments for space missions of ESA, NASA, ISRO, Roscosmos, and JAXA. He is PI of NIM and Co-PI of PEP onboard JUICE.*